Common errors in the regional atmospheric circulation simulated by the CMIP multi-model ensemble

Swen Brands[1]

[1]MeteoGalicia

November 24, 2022

Abstract

The ability of global climate models to reproduce recurrent regional atmospheric circulation types is introduced as an overarching concept to explore potential dependencies between these models. If this approach is applied on a sufficiently large spatial domain, the similarity of the resulting error pattern can be compared from one model to another. By computing a pattern correlation matrix for a large multi-model ensemble from the Coupled Model Intercomparison Project, groups of comparatively strong correlation coefficients are obtained for those models working with similar atmospheric components. Thereby, frequent shared error patterns are found within in the ensemble, which also occur for nominally different atmospheric component models.

Common errors in the regional atmospheric circulation simulated by the CMIP multi-model ensemble

Swen Brands [1]

[1]MeteoGalicia, Consellería de Medio Ambiente, Territorio y Vivienda - Xunta de Galicia, Santiago de Compostela, Spain

Key Points:

- Global Climate Models have common regional atmospheric circulation errors.
- Clusters of similar error patterns are obtained if the models are grouped according to their atmospheric sub-model.
- Common error patterns also occur for nominally different atmospheric sub-models.

Corresponding author: Swen Brands, `swen.brands@gmail.com`

Abstract

The ability of global climate models to reproduce recurrent regional atmospheric circulation types is introduced as an overarching concept to explore potential dependencies between these models. If this approach is applied on a sufficiently large spatial domain, the similarity of the resulting error pattern can be compared from one model to another. By computing a pattern correlation matrix for a large multi-model ensemble from the Coupled Model Intercomparison Project, groups of comparatively strong correlation coefficients are obtained for those models working with similar atmospheric components. Thereby, frequent shared error patterns are found within in the ensemble, which also occur for nominally different atmospheric component models.

As the number of nominally different Global Climate Models (GCMs) participating in the Coupled Model Intercomparison Project (CMIP) increases (Taylor et al., 2012; Eyring et al., 2016), so does the need to explore the degree to which they have been developed independently. This effort is important because the spread of the multi-model ensemble is assumed to provide reliable uncertainty estimates of the climate system's response to external forcing (Masson-Delmotte et al., 2021). Thus, similar development strategies, such as shared parametrization schemes or reference datasets used for model verification, would weaken the ensemble's suitability for uncertainty estimation and also compromise the use of unweighted multi-model mean averages (Masson & Knutti, 2011; Knutti et al., 2013).

Due to the complexity of the models' source code and also due to code availability restrictions, such model dependencies are commonly derived from model output data in scientific practice. One possible approach is to feed the inter-model distances of various field variables into a clustering algorithm, which then identifies shared error structures that are assumed to point to inter-model dependencies (Brunner et al., 2020).

Here it is shown that the GCMs' spatial error patterns correlate considerably if they are diagnosed in terms of their ability to reproduce the observed climatological frequency of the 27 regional atmospheric circulation types defined by Lamb (1972) and Jenkinson and Collison (1977), which can be computed for any region of the Northern Hemisphere mid-to-high latitudes (Jones et al., 2013). Calculated upon instantaneous sea-level pressure values, these *Lamb Weather Types* (LWTs) are known to be linked with a number of key variables in atmospheric physics and chemistry (Trigo & DaCamara, 2000; Hertig et al., 2020), and can thus be considered an overarching concept to describe regional-scale climate variability (Maraun et al., 2017).

The present study makes use of the 6-hourly instantaneous LWT sequences computed in Brands (2022). These time series cover the period 1979 to 2005 and are provided on a regular 2.5° grid covering a zonal belt between 35° and 70°N. They have been calculated for 2 distinct reanalyses and 56 nominally different coupled model configurations contributing historical experiments to CMIP5 and 6. For the present study, this catalogue has been extended by the ECMWF ERA5 reanalysis (Hersbach et al., 2020), here used as reference dataset, and by 4 additional GCMs, namely GFDL-ESM2G (Dunne et al., 2012), GFDL-ESM4 (Dunne et al., 2020), INM-CM5 (Volodin et al., 2017) and KACE1.0-G (Lee et al., 2019); the former participating in CMIP5 and the latter three in CMIP6, respectively. All applied LWT catalogues were permanently stored at `https://doi.org/https://doi.org/10.5281/zenodo.4452080`. An exhaustive metadata archive, including the exact run specifications and reference articles for the GCMs used here, is provided in the *get_historical_metadata.py* function stored at `https://doi.org/10.5281/zenodo.5564150`. Note that the results of the present study are almost insensitive to internal model variability arsing from initial conditions uncertainty, which is illustrated in Brands (2022), Figure 12.

At each box of the aforementioned Northern Hemisphere grid, the Mean Absolute Error (MAE) of the $n = 27$ relative LWT frequencies for a given GCM, denoted m, is calculated with respect to the respective frequencies from the reanalysis, denoted o (Brands, 2022):

$$MAE = \frac{1}{n}\Sigma_{i=1}^{n}|m_i - o_i| \tag{1}$$

, thereby obtaining 60 spatial error patterns (one for each GCM) covering the Northern Hemisphere mid-to-high latitudes. The corresponding maps can be found in the supplementary material to this article and an illustrative example displaying the results for two nominally different GCMs in shown in Figure 1. Then, the correlation matrix of these patterns is calculated in order to detect common error patterns (see Figure 2). Using the metadata collected in *get_historical_metadata.py*, those coupled model configurations sharing the same atmospheric general circulation model (*AGCM*), or versions thereof, are put into the same group and placed next to each other in the correlation matrix. This way, 12 distinct *AGCM* groups can be distinguished, each one containing at least 2 GCMs (see Table 1). Within each of these groups, the pairwise pattern correlation coefficients (rho, ×100 hereafter) do not fall below 65, except for one single pair: FGOALS-g2 and g3, pertaining to the *GAMIL AGCM* group ($rho = 47$). The remaining 11 *AGCM* groups exceed the aforementioned correlation threshold and will hereafter be referred to as AGCM *clusters* or *families*. For ease of understanding, GCM configurations are printed normal and the AGCMs used therein are printed cursive along the article.

Concerning the pattern correlation between different AGCM families, the *ECAM* cluster correlates comparatively strong with the *HadGAM/UM*, *LMDZ*, *GSMUV/MRI-AGCM* and *INM-AGCM* clusters, yielding correlation coefficients in the range of 66–75, 60–79, 59–75 and 63–82, respectively, and even stronger associations with the *GFDL-AM* family (58–89). The *ECHAM* cluster is also closely associated with *CanAM4*, i.e. the AGCM used in CanESM2 (73–82). The *HadGAM/UM* cluster yields correlation coefficients in the range of 66–80 and 62–73 with the *LMDZ* and *GFDL-AM* clusters, except for the somewhat weaker links with the *GFDL-AM* version used in KIOST-ESM (55–62). *HadGAM/UM* is also strongly linked with *CanAM4* (70–77) and with the *INM-AGCM* version used in INM-CM5 (73–80). The two BCC-CSM versions are here assigned to the *CAM* family because BCC-CSM's atmospheric component *BCC-AGCM* was originally developed from *CAM3* (Wu et al., 2010). The *CAM* family correlates comparatively strong with one half of the *ECHAM* family (MPI-ESM-LR, MPI-ESM-MR, MPI-ESM1.2-LR and MPI-ESM1.2-HR, 61–81), as well as with GFDL-CM3 and GFDL-ESM2G (62–82), and with GISS-E2.1-G (73–81). The IFS family is only moderately correlated with the remaining AGCM clusters, except for EC-Earth2.3 correlating relatively strongly with the ECHAM family. The lowest pattern correlations with the other clusters are obtained for the *MIROC-AGCM/CCSR-AGCM* family, with the exception of MIROC-ESM.

With $rho < 40$ on average (see axis labels in Figure 2), MIROC-ES2L, MIROC5 and FGOALS-g2 are the most independent coupled model versions considered here, whereas MPI-ESM-LR, MPI-ESM-MR and MPI-ESM-1.2-LR are the most dependent or, if seen the other way around, most influential GCMs ($rho > 70$). Among the institutions contributing a single model, IITM-ESM constitutes a rather independent GCM that relies on *GFS* in the atmosphere, which is not used by any other GCM. CSIRO-MK3.6 is also relatively poorly correlated with the other GCMs, but has not been further developed since CMIP5. As stated above, CanESM2's average correlation coefficient with the remaining GCMs is comparatively large.

In summary, 55 out of the 60 GCMs considered here can be grouped into 11 model families using two straightforward criteria: a common origin of the atmospheric submodel and a sufficiently large error pattern correlation with the other members of the same group.

The thereby obtained AGCM clusters yield within-group pattern correlation coefficients generally in excess of 70, which do not fall below 65 in any case. The error patterns of *distinct* AGCM families yield a comparable degree of agreement in some cases (e.g. for the ECHAM and GFDL-AM families), potentially indicating unexpected model dependencies that have not been reported so far.

Making use of the metadata archive available at `https://doi.org/10.5281/zenodo.4555367`, GCMs can be alternatively ordered according to their submodels for *other* climate system components, using appropriate alternative error measures. This effort, as well as the use of the proposed atmospheric circulation error to constrain future climate projections (Eyring et al., 2019), is left open for future studies.

Open Research

The LWT catalogues applied here have been stored at `https://doi.org/https://doi.org/10.5281/zenodo.4452080`, updated to version 4 for the present study. The underlying Python code, and particularly the *get_historical_metadata.py* function containing an extensive GCM metadata archive, has also been updated at `https://doi.org/10.5281/zenodo.4555367`. The error maps underlying Figure 2 and the exact numerical values of the correlation matrix are provided with the supplementary material to this article, available at `https://doi.org/10.6084/m9.figshare.19596535.v2`

Acknowledgments
I would like to thank the research institutes participating in CMIP for sharing the GCM data analysed here and also appreciate the public availability of the ECMWF ERA5 reanalysis dataset.

References

Brands, S. (2022). A circulation-based performance atlas of the CMIP5 and 6 models for regional climate studies in the Northern Hemisphere mid-to-high latitudes. *Geoscientific Model Development*, *15*(4), 1375–1411. doi: https://doi.org/10.5194/gmd-15-1375-2022

Brunner, L., Pendergrass, A. G., Lehner, F., Merrifield, A. L., Lorenz, R., & Knutti, R. (2020). Reduced global warming from CMIP6 projections when weighting models by performance and independence. *Earth System Dynamics*, *11*(4), 995–1012. doi: https://doi.org/10.5194/esd-11-995-2020

Dunne, J. P., Horowitz, L. W., Adcroft, A. J., Ginoux, P., Held, I. M., John, J. G., ... Zhao, M. (2020). The GFDL Earth System Model version 4.1 (GFDL-ESM 4.1): Overall coupled model description and simulation characteristics. *Journal of Advances in Modeling Earth Systems*, *12*(11), e2019MS002015. doi: https://doi.org/10.1029/2019MS002015

Dunne, J. P., John, J. G., Adcroft, A. J., Griffies, S. M., Hallberg, R. W., Shevliakova, E., ... Zadeh, N. (2012). GFDL's ESM2 Global Coupled Climate-Carbon Earth System Models. Part I: Physical formulation and baseline simulation characteristics. *Journal of Climate*, *25*(19), 6646–6665. doi: https://doi.org/10.1175/JCLI-D-11-00560.1

Eyring, V., Bony, S., Meehl, G. A., Senior, C. A., Stevens, B., Stouffer, R. J., & Taylor, K. E. (2016). Overview of the Coupled Model Intercomparison Project Phase 6 (CMIP6) experimental design and organization. *Geoscientific Model Development*, *9*(5), 1937–1958. doi: https://doi.org/10.5194/gmd-9-1937-2016

Eyring, V., Cox, P., Flato, G., Gleckler, P., Abramowitz, G., Caldwell, P., ... Williamson, M. (2019). Taking climate model evaluation to the next level. *Nature Climate Change*, *9*, 102-110. doi: https://doi.org/10.1038/s41558-018-0355-y

Hersbach, H., Bell, B., Berrisford, P., Hirahara, S., Horányi, A., Muñoz-Sabater, J., ... Thépaut, J.-N. (2020). The ERA5 global reanalysis. *Quarterly Journal of the Royal Meteorological Society*, *146*(730), 1999-2049. doi: https://doi.org/10.1002/qj.3803

Hertig, E., Russo, A., & Trigo, R. M. (2020). Heat and ozone pollution waves in central and south Europe—characteristics, weather types, and association with mortality. *Atmosphere*, *11*(12), 1271. doi: https://doi.org/10.3390/atmos11121271

Jenkinson, A., & Collison, F. (1977). *An initial climatology of gales over the North Sea* (Vol. 62; Tech. Rep. No. 18). Bracknell, UK: Meterololgical Office.

Jones, P. D., Harpham, C., & Briffa, K. R. (2013). Lamb weather types derived from reanalysis products. *International Journal of Climatology*, *33*(5), 1129-1139. doi: https://doi.org/10.1002/joc.3498

Knutti, R., Masson, D., & Gettelman, A. (2013). Climate model genealogy: Generation CMIP5 and how we got there. *Geophysical Research Letters*, *40*(6), 1194-1199. doi: https://doi.org/10.1002/grl.50256

Lamb, H. (1972). British isles weather types and a register of daily sequence of circulation patterns, 1861-1971. *Geophysical Memoir*, *116*, 85pp. (HMSO)

Lee, J., Kim, J., Sun, M.-A., Kim, B.-H., Moon, H., Sung, H. M., ... Byun, Y.-H. (2019, 08). Evaluation of the Korea Meteorological Administration Advanced Community Earth-System model (k-ace). *Asia-Pacific Journal of Atmospheric Sciences*, *56*, 381–395. doi: https://doi.org/10.1007/s13143-019-00144-7

Maraun, D., Shepherd, T., Widmann, M., Zappa, G., Walton, D., Gutiérrez, J., ... Mearns, L. (2017). Towards process-informed bias correction of climate change simulations. *Nature Climate Change*, *7*, 764-773. doi: https://doi.org/10.1038/nclimate3418

Masson, D., & Knutti, R. (2011). Climate model genealogy. *Geophysical Research Letters*, *38*(8), L08703. doi: https://doi.org/10.1029/2011GL046864

Masson-Delmotte, V., et al. (Eds.). (2021). *Climate Change 2021: The Physical Science Basis. Contribution of Working Group I to the Sixth Assessment Report of the Intergovernmental Panel on Climate Change.* Cambridge University Press.

Taylor, K. E., Stouffer, R. J., & Meehl, G. A. (2012). An overview of CMIP5 and the experiment design. *Bulletin of the American Meteorological Society*, *93*(4), 485-498. doi: https://doi.org/10.1175/BAMS-D-11-00094.1

Trigo, R. M., & DaCamara, C. C. (2000). Circulation weather types and their influence on the precipitation regime in Portugal. *International Journal of Climatology*, *20*(13), 1559-1581. doi: https://doi.org/10.1002/1097-0088

Volodin, E., Mortikov, E., Kostrykin, S., Galin, V., Lykossov, V., Gritsun, A., … Iakovlev, N. (2017). Simulation of the present-day climate with the climate model INMCM5. *Climate Dynamics*, *49*, 3715–3734. doi: https://doi.org/10.1007/s00382-017-3539-7

Wu, T., Yu, R., Zhang, F., Wang, Z., Dong, M., Wang, L., … Li, L. (2010). The Beijing Climate Center atmospheric general circulation model: Description and its performance for the present-day climate. *Climate Dynamics*, *34*, 123-147. doi: https://doi.org/10.1007/s00382-008-0487-2

Table 1. Atmospheric general circulation model groups and coupled model configurations they are used in. GCMs belong to the same *cluster* if their AGCM is from the same group and if the pattern correlation coefficients with the remaining members of this group exceeds 65 (see Figure 2). Only 5 of the 60 considered GCMs cannot be grouped this way, either because their within-group pattern correlations are too low (this is the case for FGOALS-g2 and g3) or because their AGCM is unique within the multi-model ensemble considered here (this is the case for CanESM2, IITM-ESM and CSIRO-MK3.6).

AGCM group	**Coupled model configurations**
	GCMs fulfilling the grouping criteria (55)
HadGAM/UM	ACCESS1.0, ACCESS1.3, ACCESS-CM2, ACCESS-ESM1, HadGEM2-CC, HadGem2-ES, Hadgem3-GC31-MM, KACE1.0-G
ECHAM	MPI-ESM-LR, MPI-ESM-MR, MPI-ESM1.2-LR, MPI-ESM1.2-HR, MPI-ESM-1-2-HAM, AWI-ESM-1-1-LR, NESM3, CMCC-CM
CAM	CMCC-CM2-SR5, CMCC-ESM2, CCSM4, NorESM1-M, NorESM2-LM, NorESM2-MM, SAM0-UNICON, TaiESM1, BCC-CSM1.1, BCC-CSM2-MR
ARPECHE	CNRM-CM5, CNRM-CM6-1, CNRM-CM6-1-HR, CNRM-ESM2-1
IFS	EC-Earth2.3, EC-Earth3, EC-Earth3-Veg, EC-Earth3-Veg-LR, EC-Earth3-AerChem, EC-Earth3-CC
GFDL-AM	GFDL-CM3, GFDL-ESM2G, GFDL-CM4, GFDL-ESM4, KIOST-ESM
GISS-E2	GISS-E2-H, GISS-E2-R, GISS-E2.1-G
LMDZ	IPSL-CM5A-LR, IPSL-CM5A-MR, IPSL-CM6A-LR
MIROC-AGCM/CCSR AGCM	MIROC5, MIROC-ESM, MIROC6, MIROC-ES2L
GSMUV/MRI-AGCM	MRI-ESM1, MRI-ESM2.0
INM-AM	INM-CM4, INM-CM5
	GCMs not fulfilling the grouping criteria (5)
GAMIL	FGOALS-g2, FGOALS-g3
CSIRO-AGCM	CSIRO-MK3.6
CanAM	CanESM2
GFS	IITM-ESM

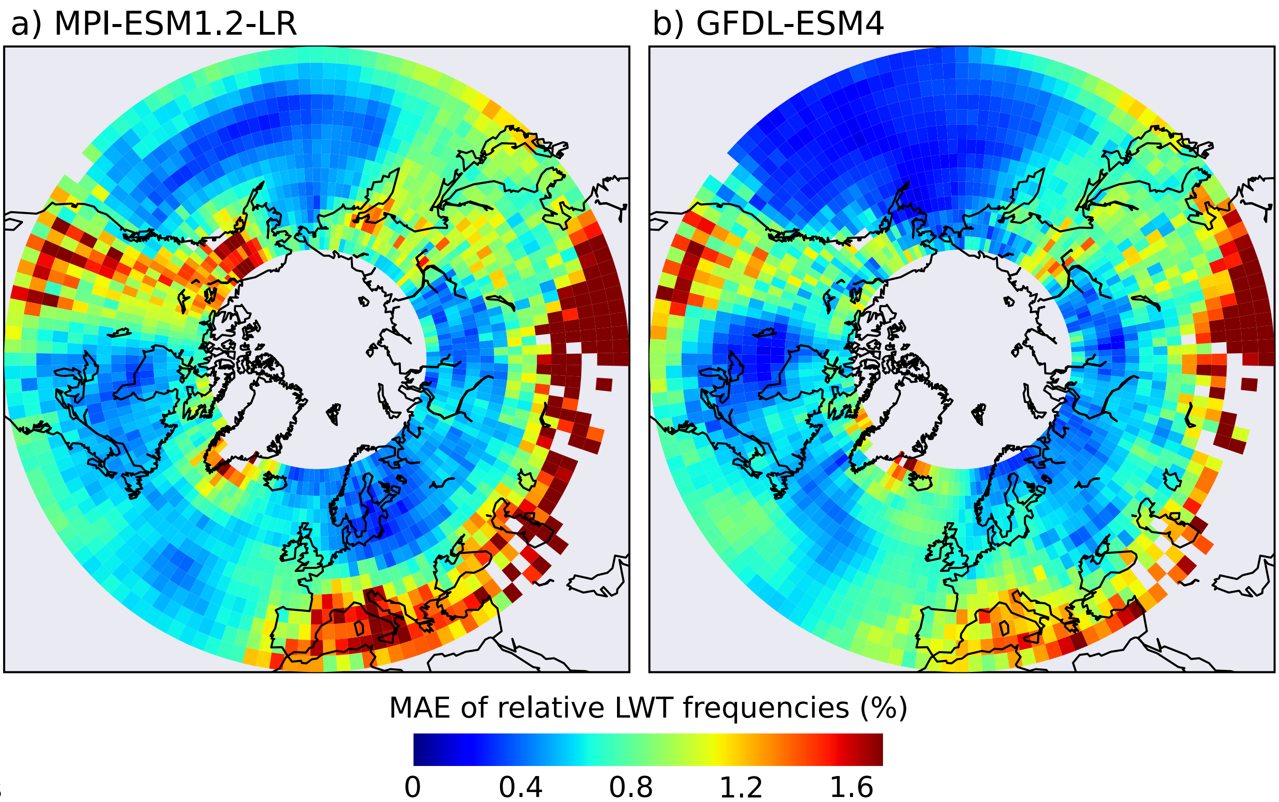

Figure 1. Spatial pattern of the Mean Absolute Error (MAE) in the relative frequencies of the 27 *Lamb Weather Types* in the Northern Hemisphere mid-to-high latitudes for a) MPI-ESM1.2-LR and b) GFDL-ESM4 over the period 1979-2005. Model errors are with respect to ERA5. The pattern correlation coefficient ($\times 100$) for this GCM pair is 79.

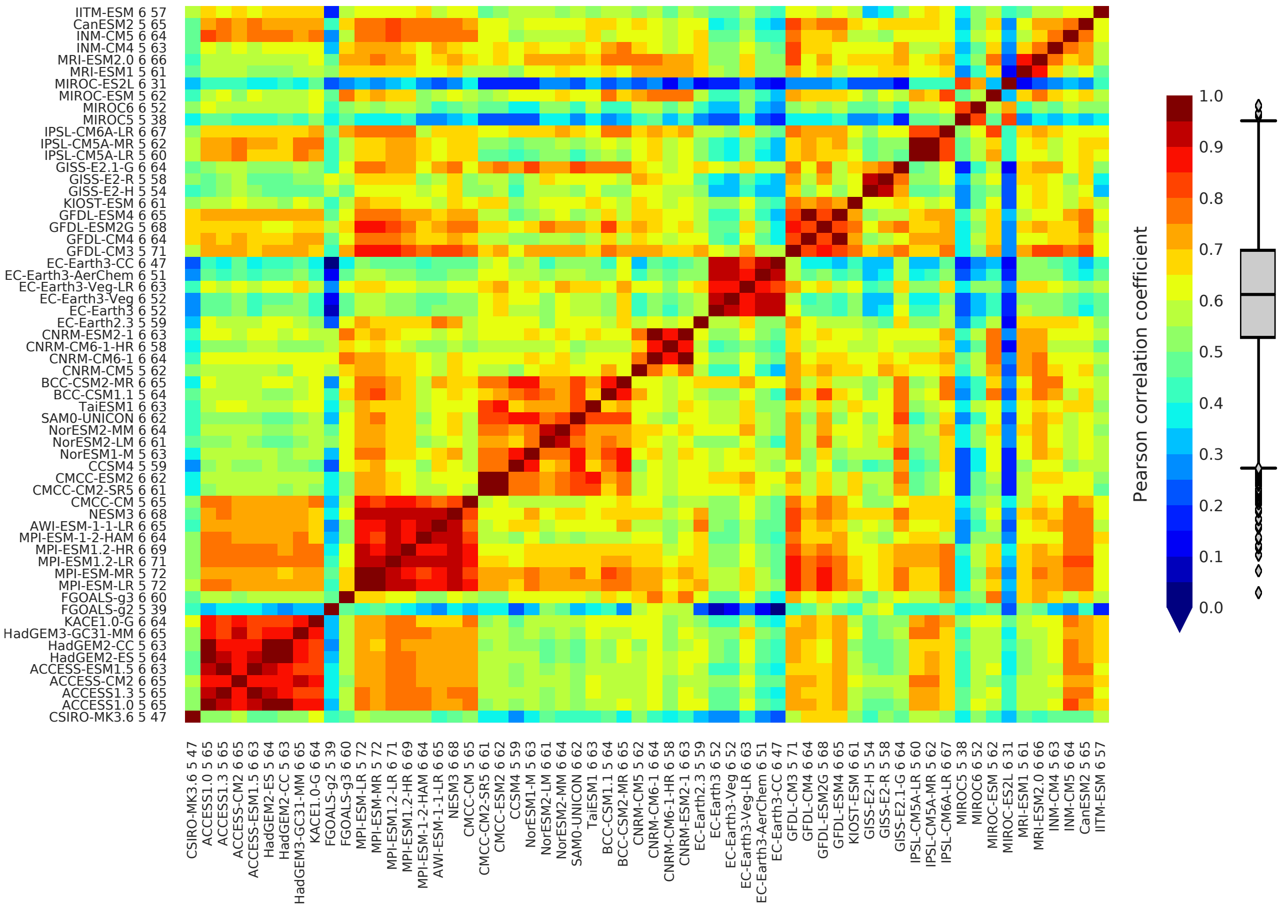

Figure 2. Spatial correlation of the Northern Hemisphere pattern of the Mean Absolute Error (MAE) in the relative frequencies of the 27 *Lamb Weather Types* for 60 distinct GCMs from CMIP5 and 6. The corresponding maps are provided in the supplementary material. The acronym, CMIP generation and average spatial correlation coefficient ($\times 100$) of each GCM are provided along the axes. The boxplot to the right of the colorbar describes the distribution of the correlation coefficients for one half of the matrix and excluding the unity values along the diagonal. The boxplot is constructed with the median, interquartile range (IQR) and whiskers of this sample, the latter placed at the 25^{th} percentile - 1.5 $\times$ IQR and at the 75^{th} percentile + $1.5 \times IQR$. Model errors are with respect to ERA5.